Rapid Communications   **Featured in Physics**

Pulse generation scheme for flying electromagnetic doughnuts

Nikitas Papasimakis,[1] Tim Raybould,[1] Vassili A. Fedotov,[1] Din Ping Tsai,[2] Ian Youngs,[3] and Nikolay I. Zheludev[1,4]

[1]*Optoelectronics Research Centre and Centre for Photonic Metamaterials, University of Southampton,*
Southampton SO17 1BJ, United Kingdom
[2]*Department of Physics, National Taiwan University and Research Center for Applied Sciences, Academia Sinica, Taipei 10617, Taiwan*
[3]*DSTL, Porton Down, Salisbury, SP4 0JQ, United Kingdom*
[4]*The Photonics Institute and Centre for Disruptive Photonic Technologies, SPMS, Nanyang Technological University, Singapore 637371*

Transverse electromagnetic plane waves are fundamental solutions of Maxwells equations. It is less known that a radically different type of solutions has been described theoretically, but has never been realized experimentally, that exist only in the form of short bursts of electromagnetic energy propagating in free space at the speed of light. They are distinguished from transverse waves by a doughnutlike configuration of electric and magnetic fields with a strong field component along the propagation direction. Here, we demonstrate numerically that such flying doughnuts can be generated from conventional pulses using a singular metamaterial converter designed to manipulate both the spatial and spectral structure of the input pulse. The ability to generate flying doughnuts is of fundamental interest, as they shall interact with matter in unique ways, including nontrivial field transformations upon reflection from interfaces and the excitation of toroidal response and anapole modes in matter, hence offering opportunities for telecommunications, sensing, and spectroscopy.

Electromagnetic waves propagating in free space are described by the source-free Maxwells equations. Examples include the vast majority of waveforms employed in optical science, such as plane waves, Bessel beams, X-waves, Airy and Gaussian pulses. The electromagnetic fields of such solutions are typically transverse to the propagation direction, and they can be written as a product of space- and time-dependent functions. However, there is a very different family of exact solutions to Maxwells equations, where the spatial and temporal structure are inherently linked and cannot be separated. Early work by Brittingham introduced the so-called focus wave modes, pulses that propagate without diffraction but carry infinite energy [1]. Soon after Richard Ziolkowski addressed this issue by considering superpositions of the original focus wave modes resulting in finite energy pulses, termed electromagnetic directed energy pulse trains (EDEPTs) [2,3]. This family of pulses and its derivatives include a wide range of exotic waveforms, such as the modified power spectrum pulse [2], nondiffracting pulses with azimuthal dependence [4,5], focused pancake pulses [6–8], and the flying doughnut (FD) pulses [9].

Flying doughnuts are single-cycle pulses, distinguished by a doughnutlike configuration of electric and magnetic fields, which feature strong longitudinal field components parallel to the pulse propagation direction [see Fig. 1(a)]. Importantly, due to the unique spatiotemporal coupling, such pulses are exceptionally broadband. Potential applications of FD pulses include particle acceleration [9], while nontrivial interactions with interfaces have been predicted [10]. In particular, owing to the topological similarity with the toroidal dipolar excitation and the presence of longitudinal field components, it has been shown that FD pulses can excite strong toroidal modes in dielectric particles, as well as anapoles, namely nonradiating combinations of electric and toroidal dipoles [11].

However, due to the complexity of the electromagnetic field configuration, broad bandwidth, and complex spatial and temporal coupling, FD pulses have not been realized to date. Early works have suggested various generation schemes based on antenna arrays, where each element in the array is considered to be driven by an electrical signal with different amplitude and temporal shape [12,13]. In this case, the electromagnetic fields radiated by all antennas in the array combine in the far-field forming the desired pulse. Nevertheless, such approaches require active control of individual radiating elements at time scales comparable to the duration of the pulse. Hence, they require complex configurations, particularly when large numbers of radiating elements are required, and cannot be translated to optical frequencies. Here, drawing on recent advances in the field of metamaterials for dispersion [14,15] and wavefront control [16–18], we introduce a method for the generation of FDs. Our approach does not require active control of individual radiating elements and can be readily adapted for the generation of other types of exotic pulses with complex spatiotemporal structure, such as localized waves [19] or variants of the FD pulse possessing orbital angular momentum [4,5].

The FD pulse exists in two different forms termed transverse electric (TE) and transverse magnetic (TM). In the case of a TE FD pulse propagating along the z axis and coming into focus at $z = 0$, $t = 0$, the electric and magnetic fields are given by (in the cylindrical coordinates ρ, θ, z) [9]:

$$E_\theta = -4if_0\sqrt{\frac{\mu_0}{\epsilon_0}}\rho\frac{q_1 + q_2 - 2ict}{[\rho^2 + (q_1 + i(z - ct))(q_2 - i(z + ct))]^3}$$

$$H_\rho = 4if_0\rho\frac{-q_1 + q_2 - 2iz}{[\rho^2 + (q_1 + i(z - ct))(q_2 - i(z + ct))]^3}$$
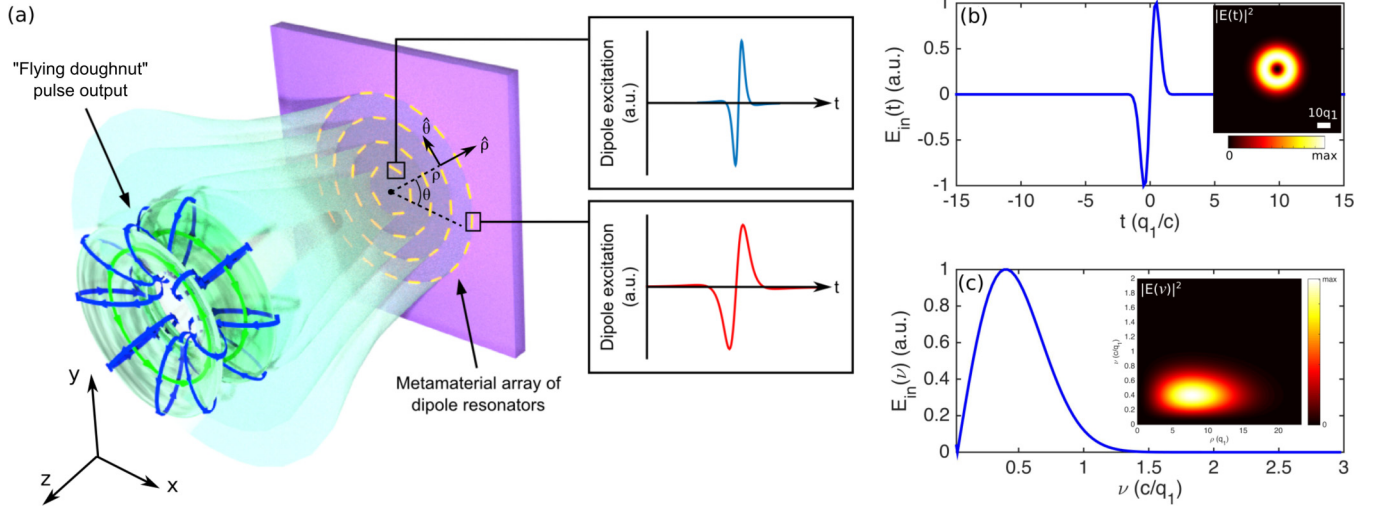
FIG. 1. (a) Schematic of a metamaterial generator of flying doughnut pulses. Concentric rings of azimuthally oriented linear dipole resonators with spatially and frequency dependent scattering properties lead to the emission of a toroidal single-cycle flying doughnut pulse. The resonators in different rings exhibit a different frequency dispersion (see insets). (b), (c) The temporal (b) and frequency (c) form of the single-cycle radially polarized pulse driving the metamaterial generator. Inset to (b) shows the electric field intensity profile of the input pulse in the xy plane (transverse to the propagation direction). Inset to (c) shows the spectral power of the input pulse at different distances from the pulse center.

$$H_z = -4f_0 \frac{\rho^2 - (q_1 + i(z - ct))(q_2 - i(z + ct))}{[\rho^2 + (q_1 + i(z - ct))(q_2 - i(z + ct))]^3}, \quad (1)$$

where f_0 is an arbitrary normalization constant. The parameters q_1 and q_2 have the dimensions of length and represent the effective wavelength of the pulse and the focal region depth, respectively. Beyond the focal region ($z > q_2$), the FD diffracts in the same manner as a Gaussian pulse with wavelength q_1 and Rayleigh length $q_2/2$. Owing to the duality of Maxwells equations in free space, the TM solutions are readily obtained by interchanging electric and magnetic field components. As is evident from Eqs. (1), the FD pulse is a nonseparable solution to Maxwells source-free equations meaning that it cannot be written as a product of a space-dependent and a time-dependent function. Here, we focus on the generation of TE FD pulses.

The generation of FD pulses presents a number of substantial challenges. For example, the broad frequency spectrum of the pulse requires a broadband source, while the frequency content of the pulse varies substantially along the radial direction [Fig. 1(c)]. We address these challenges by introducing a new class of gradient metamaterials that allow simultaneous spatial and temporal wavefront manipulations and are based on low Q-factor dipole resonators (see Supplemental Material [20]). We employ a cylindrically symmetric metamaterial array [see schematic representation in Fig. 1(a)], reflecting the symmetry of the FD pulse. The array consists of azimuthally oriented electric dipoles arranged in concentric rings. The spatiotemporal coupling is provided by varying the properties of the metamaterial elements across the radial direction according to the parameters of the targeted FD pulse (effective wavelength q_1 and Rayleigh length q_2). We consider illumination by an ultrashort Gaussian, azimuthally polarized pulse and calculate numerically the electromagnetic fields emitted by the array. Such azimuthally polarized pulses can be readily generated in the optical range in a number of ways, including beam interference [21], segmented waveplates [22] and, more recently,

by dielectric metasurfaces [23]. They provide the required field topology and bandwidth for the generation of FD pulses. In contrast to the targeted FD pulses, they are space-time separable and can be described approximately by [24]:

$$\vec{E}_{in}(\rho, \theta, t) = \hat{\theta} E_0 \mathrm{P}(\rho) \mathrm{T}(t) \quad (2)$$

with

$$\mathrm{P}(\rho) = \frac{\rho e^{(-\rho/s)^2}}{s} \quad (3)$$

$$\mathrm{T}(t) = sin(\omega_{in} t) e^{-\frac{\ln 2(2t/\tau_{in})^2}{2}}, \quad (4)$$

where E_0 is an arbitrary constant defining the energy of the pulse, s is the waist, ω_{in} is the carrier frequency, and τ_{in} is the duration of the pulse. The waist of the pulse is defined such that it is equal to that of the target FD pulse. The carrier frequency is matched to the peak frequency of the target FD pulse, while the time duration of the input pulse is chosen to provide a single-cycle pulse with a bandwidth close to the FD pulse bandwidth. The transverse profile of the input pulse is shown in the inset to Fig. 1(b). In a frequency representation, the input pulse can be written as:

$$\vec{E}_{in}(\rho, \theta, \omega) = \hat{\theta} E_0 \mathrm{P}(\rho) \Omega(\omega) \quad (5)$$

with

$$\Omega(\omega) = \int e^{i\omega t} \mathrm{T}(t) dt. \quad (6)$$

The pulse generator for TE FD pulses consists of an array of 217 azimuthally polarized point dipole scatterers, with prescribed frequency dependent radiation patterns, arranged in ten concentric rings [see schematic in Fig. 1(a)]. The metamaterial structure is cylindrically symmetric with dipole scatterers in the same ring being identical. In particular, dipoles in the ring of radius ρ_i respond to an azimuthally polarized electric field according to their frequency dependent complex polarizability
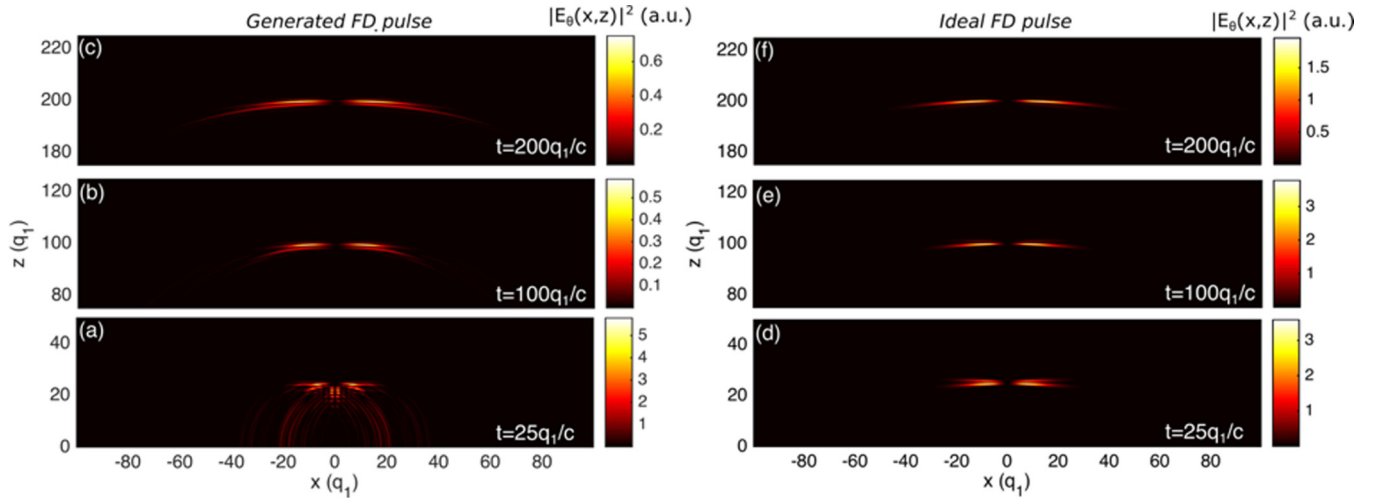
FIG. 2. Snapshots of the generated (a)–(c) and ideal (d)–(f) FD pulse at three different moments in time ($t = 25q_1/c$, $100q_1/c$, and $200q_1/c$) with $q_2 = 300q_1$. Color maps show the modulus squared of the azimuthal (normal to the xz plane) electric field. Electric field units are consistent between (a)–(c) and between (d)–(f).

$\alpha_i(\omega)$. Here we are concerned with $\lambda/2$ resonators, hence their spectral response can be described by a Lorentzian centered at frequency $\omega_{o,i}$ with a decay rate γ_i. These parameters can be controlled by the length and width of the dipole resonators (see Ref. [20], Fig. S1). The peak frequency and bandwidth of the dipole scatterers vary radially following the profile of the target FD pulse. As a result, the dipoles near the center emit shorter pulses at higher frequencies [see top inset to Fig. 1(a)] compared to the dipoles at the periphery of the array [see bottom inset to Fig. 1(a)]. Our calculations are based on a point dipole model, where each resonator in the array is replaced by a point dipole scatterer with the same resonant polarizability (obtained by COMSOL modeling, see Supplemental Material [20]).

A dipole at position $\vec{r}_i = (\rho_i, \theta_i, 0)$ in the array (assuming the array lies in the $z = 0$ plane) is excited by the electric field of the input azimuthally polarized pulse at this site, $\vec{E}_{in}(\rho_i, \theta_i, \omega) = \vec{E}_{in,i}(\omega)$. Taking into account the cylindrical symmetry of the system and the fact that both the dipole resonators and the incident electric field are oriented azimuthally, the induced electric dipole moment is:

$$\vec{p}_i(\omega) = \alpha_i(\omega)\vec{E}_{in,i}(\omega). \tag{7}$$

At each frequency, ω, the field scattered by dipole $\vec{p}_i$ at an observation point r_o is calculated by:

$$\vec{E}_{sc,i}(\vec{r}_o, \omega) = \frac{k^2 e^{ik|\vec{R}_i| - i\omega t}}{4\pi\epsilon_0 |\vec{R}_i|^3}\vec{R}_i \times \vec{p}_i(\omega) \times \vec{R}_i, \tag{8}$$

where $k = \omega/c$, c is the speed of light in vacuum, and $\vec{R}_i = \vec{r}_o - \vec{r}_i$. The total field at point $\vec{r}_o$ scattered by all dipoles in the array is:

$$\vec{E}_{sc}(\vec{r}_o, \omega) = \sum_i \vec{E}_{sc,i}(\vec{r}_o, \omega). \tag{9}$$

After a Fourier transform, we obtain the scattered pulse in the time domain in the form:

$$\vec{E}_{sc}(\vec{r}_o, t) = \frac{1}{2\pi}\int e^{-i\omega t}\vec{E}_{sc}(\vec{r}_o, \omega)d\omega. \tag{10}$$

Following the procedure outlined above, we target a TE FD pulse with effective wavelength q_1, Rayleigh length $q_2 = 300q_1$, which is focused at $z_0 = 0$ and $t_0 = 0$. The results of our calculations are presented in Fig. 2, where the azimuthally polarized electric field is presented both for the ideal (target) FD pulse and the metamaterial-generated pulse at three different moments in time. As shown in Fig. 2(a), shortly after the excitation of the metamaterial surface with the radially polarized pulse, a few-cycle pulse is emitted with a wavefront that features strong side lobes and a tail close to the center of the pulse. However, upon propagation these inhomogeneities of the wavefront are rapidly damped due to diffraction [Fig. 2(b)], and after a propagation distance of $z = 200q_1$, the pulse acquires a toroidal shape consisting of a single cycle [Fig. 2(c)]. Moreover, the values of the electric field intensity for propagation distances between $z = 100q_1$ and $z = 200q_1$ remain almost constant, indicating the weakly diffracting behavior of the generated pulse. As the propagation distance increases, the electric field profile of the generated pulse [Figs. 2(a)–2(c)] converges to that of the target pulse [Figs. 2(d)–2(f)] with both pulses diffracting in a similar way. An important difference here, however, is that the ideal FD pulse experiences shape changes due to Gouy phase shifts, with the pulse duration increasing from 1 to 1 1/2 cycles. Such changes are much less pronounced in the case of the generated pulse.

One of the fascinating properties of the FD pulse is its space-time nonseparability, which leads to a spatially varying frequency spectrum. This is in sharp contrast to the case of the input driving pulse, which is space-time separable and its frequency spectrum is uniform throughout the pulse wavefront. In our approach, the space-time nonseparability is induced by the gradient structure of the metamaterial generator. The frequency spectra of the generated and target pulses are shown in Fig. 3 at three different propagation distances. Close to the metamaterial generator [Fig. 3(a)], the frequency spectrum of the generated pulse deviates significantly from that of the target pulse [Fig. 3(d)] due to the presence of strong near-field contributions. However, the space-time nonseparability can already be seen in the central part of its spectrum, which
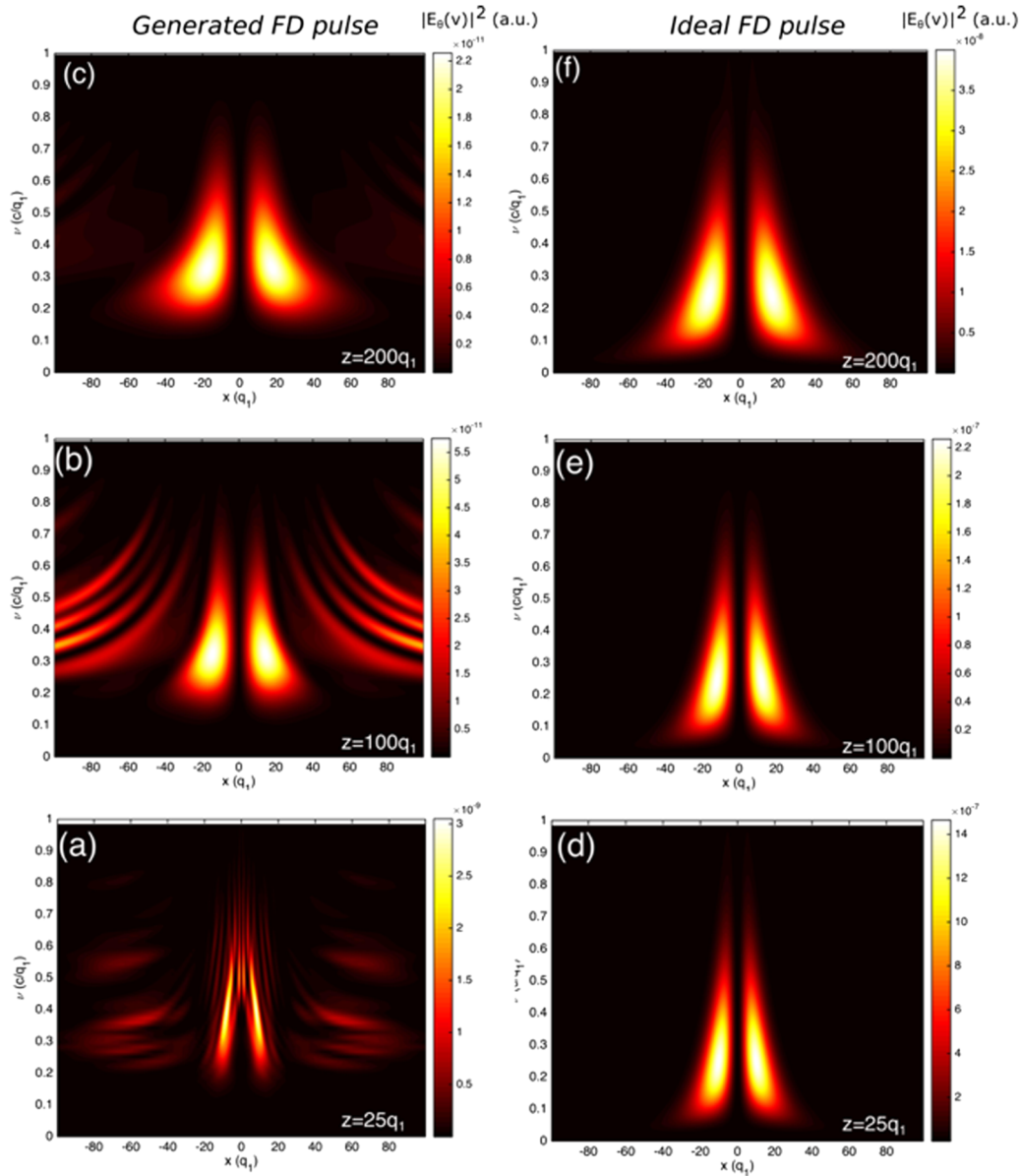
FIG. 3. Spatially varying spectra of the generated (a)–(c) and ideal (d)–(f) FD pulse at three different distances from the metamaterial generator ($z = 25q_1$, $100q_1$, and $200q_1$) with $q_2 = 300q_1$. Color maps show the modulus squared of the azimuthal (normal to the xz plane) electric field.

begins to resemble the spectrum of the target FD. As the pulses propagate further ($z = 100q_1$), the similarity between their spectra increases [Figs. 3(b) and 3(e)], although, due to diffraction, the side lobes of the generated pulse can still be clearly observed at the periphery. At a propagation distance of $z = 200q_1$, these side lobes are all but absent and the generated pulse assumes a form very close to that of an FD pulse. Here, the peak frequency, ν_{max}, in the spectrum of the generated pulse is strongly position dependent varying from $\nu_{max} \simeq 0.35c/q_1$ close to the center of the pulse to $\nu_{max} \simeq 0.2c/q_1$ at the outer areas of the pulse. We would like to note that the metamaterial FD generator does not introduce any changes in the topology of the pulse: Both the input radially polarized pulse and the output FD pulse exhibit a singularity at their respective centers. Rather, the main role of the FD generator is to introduce coupling of the spatial and temporal structure of the pulse.

To quantify the similarity of the generated FD pulse to its target form, we introduce a frequency dependent figure of merit (FOM) based on the spatial overlap of the azimuthal electric fields of the two pulses:

$$\text{FOM}(\nu) = \left| \frac{\int E_{gen}(\nu) E_{ideal}(\nu) dr^3}{\sqrt{\int |E_{gen}(\nu)|^2 dr^3 \int |E_{ideal}(\nu)|^2 dr^3}} \right|. \quad (11)$$

Owing to the normalization of FOM, values close to null indicate low similarity between the pulses, whereas values close to unity indicate good match between the pulses. In Fig. 4(a), we present FOM at three different propagation distances, corresponding to the frequency spectra in Figs. 3(a)–3(c). Close to the metamaterial generator [black dashed line in Fig. 4(a)], the FOM exhibits strong spectral mismatch, especially for high frequency components. This is a
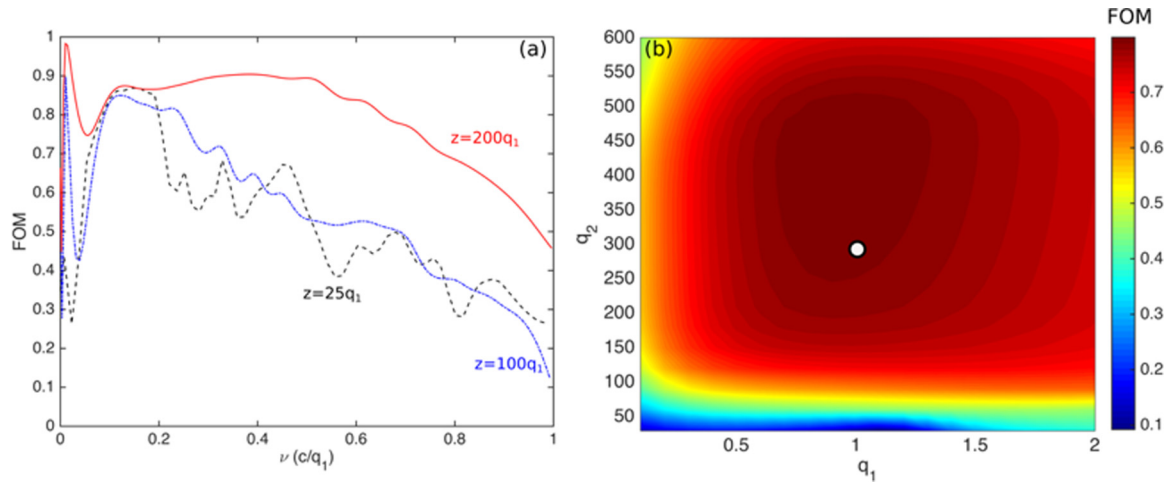
FIG. 4. (a) Frequency dependent figure of merit (FOM), defined as the spatial overlap of the generated pulse and the ideal (target) pulse at each frequency [Eq. (11)]. Dashed black, dash-dot blue, and solid red lines correspond to three different propagation distances $z = 25q_1$, $100q_1$, and $200q_1$, respectively. (b) FOM calculated and averaged over all frequencies for different q_1 and q_2 parameters of the ideal FD pulse. The white circle marks the values of q_1 and q_2 parameters initially targeted in our study.

direct result of the appearance of side lobes, which significantly distort the wavefront of the generated pulse. However, at longer propagation distances [red solid line in Fig. 4(a)], the FOM value exceeds 0.7, which indicates a high degree of similarity between the generated and target pulses both in terms of topology as well as spectral content. To further demonstrate that the generated pulse resembles closely the target FD pulse (rather than just an FD pulse), we performed a parametric scan, calculating the spatial overlap between the two pulses while varying the values of q_1 and q_2. As shown in Fig. 4(b), the highest values of FOM occur close to the parameters of the target FD, hence validating our approach.

In conclusion, we have introduced a type of metamaterials that allows complex spatiotemporal manipulations of electromagnetic waves and have demonstrated numerically the generation of flying doughnut pulses. Our approach is based on metamaterial arrays of electric dipole resonators with orientation, resonance frequency, and linewidth that vary spatially throughout the array, and hence FD generators can be readily realized with plasmonic or dielectric metasurfaces. In the latter case, in particular, near unity transmittance and reflectance has been recently observed [23,25], which enables the realization of FD generators with high conversion efficiency. FD pulses constitute a new type of broadband information carrier confined both in time and space, and as such they can be employed in telecommunications applications. Here, the nonseparability of the FD pulse time and space dependence should allow the transmission of information over FD-specific channels, which can be distinguished from the conventional case of

space- and time-separable pulses. Moreover, the space-time nonseparability property of FD pulses enables the encoding of information about the spectral (or, equivalently, temporal) form of the pulse, into its wavefront, and vice versa. This opens up intriguing properties for the spectroscopy and characterization of materials properties, where one could acquire spectral information simply through imaging the pulse wavefront, eliminating the need for spectrometers or monochromators. Conversely, information about the spatial shape of the pulse can be obtained through spectral measurements. Our approach provides a route towards the generation of FD pulses at arbitrary frequency ranges (in particular THz/optical), which will be crucial in enabling such spectroscopic applications. Finally, such pulses can be considered as the propagating counterparts of the recently observed localized toroidal excitations in matter [26]. They have also been shown to excite toroidal dipole and anapole modes in dielectric particles [10,11], providing thus the basis for toroidal-specific forms of spectroscopy.

[1] J. N. Brittingham, J. Appl. Phys. **54**, 1179 (1983).

[2] R. W. Ziolkowski, J. Math. Phys. **26**, 861 (1985).

[3] R. W. Ziolkowski, Phys. Rev. A **39**, 2005 (1989).

[4] J. Lekner, J. Opt. A - Pure Appl. Op. **6**, 711 (2004).

[5] J. Lekner, J. Opt. A - Pure Appl. Op. **6**, L29 (2004).

[6] S. Feng, H. G. Winful, and R. W. Hellwarth, Opt. Lett. **23**, 385 (1998).

[7] S. Feng, H. G. Winful, and R. W. Hellwarth, Phys. Rev. E **59**, 4630 (1999).

[8] S. Hunsche, S. Feng, H. G. Winful, A. Leitenstorfer, M. C. Nuss, and E. P. Ippen, J. Opt. Soc. Am. A **16**, 2025 (1999).

[9] R. W. Hellwarth and P. Nouchi, Phys. Rev. E **54**, 889 (1996).

[10] T. Raybould, V. Fedotov, N. Papasimakis, I. Youngs, and N. Zheludev, Opt. Express **24**, 3150 (2016).

[11] T. Raybould, V. A. Fedotov, N. Papasimakis, I. Youngs, and N. I. Zheludev, Appl. Phys. Lett. **111**, 081104 (2017).

[12] R. Ziolkowski, IEEE Trans. Antennas Propag. **40**, 888 (1992).

[13] A. M. Shaarawi, I. M. Besieris, R. W. Ziolkowski, and S. M. Sedky, J. Opt. Soc. Am. A **12**, 1954 (1995).

[14] N. Papasimakis, V. A. Fedotov, N. I. Zheludev, and S. L. Prosvirnin, Phys. Rev. Lett. **101**, 253903 (2008).

[15] B. Luk'yanchuk, N. I. Zheludev, S. A. Maier, N. J. Halas, P. Nordlander, H. Giessen, and C. T. Chong, Nat. Mater. **9**, 707 (2010).

[16] N. Yu, P. Genevet, M. A. Kats, F. Aieta, J. P. Tetienne, F. Capasso, and Z. Gaburro, Science **334**, 333 (2011).

[17] X. Ni, N. K. Emani, A. V. Kildishev, A. Boltasseva, and V. M. Shalaev, Science **335**, 427 (2012).

[18] V. A. Fedotov, J. Wallauer, M. Walther, M. Perino, N. Papasimakis, and N. I. Zheludev, Light Sci. Appl. **4**, e306 (2015).

[19] H. E. Hernández-Figueroa, M. Zamboni-Rached, and E. Recami, *Localized Waves* (J. Wiley & Sons, New York, 2007).

[20] See Supplemental Material at http://link.aps.org/supplemental/10.1103/PhysRevB.97.201409 for more details on the FD generator design and the spatiotemporal shape of the generated pulses.

[21] S. C. Tidwell, D. H. Ford, and W. D. Kimura, Appl. Opt. **29**, 2234 (1990).

[22] R. Dorn, S. Quabis, and G. Leuchs, Phys. Rev. Lett. **91**, 233901 (2003).

[23] S. Kruk, B. Hopkins, I. Kravchenko, A. Miroshnichenko, D. N. Neshev, and Y. S. Kivshar, Appl. Phys. Lett. **1**, 030801 (2016).

[24] R. Oron, S. Blit, N. Davidson, A. A. Friesem, Z. Bomzon, and E. Hasman, Appl. Phys. Lett. **77**, 3322 (2000).

[25] P. Moitra, B. A. Slovick, W. li, I. I. Kravchencko, D. P. Briggs, S. Krishnamurthy, and J. Valentine, ACS Photonics **2**, 692 (2015).

[26] N. Papasimakis, V. A. Fedotov, V. Savinov, T. A. Raybould, and N. I. Zheludev, Nat. Mater. **15**, 263 (2016).